

# A high sensitivity two-color interferometer for pulsed power plasmas<sup>a)</sup>

B. V. Weber

Plasma Physics Division, Naval Research Laboratory, Washington, DC 20375

S. F. Fulghum

Science Research Laboratory, Somerville, Massachusetts 02143

(Presented on 14 May 1996)

A high sensitivity, high bandwidth, two-color interferometer (1064 and 532 nm) has been tested on the Hawk pulsed power generator at the Naval Research Laboratory. The phase resolution is  $10^{-5}$  waves with a rise time of 3 ns, a new capability for diagnosing plasmas, and neutrals in pulsed power experiments. The two-color feature is used to distinguish phase shifts from free (plasma) electrons and bound (neutral and ion) electrons. Simultaneous electron and neutral density measurements were demonstrated in a plasma opening switch (POS) experiment. The ability to measure small phase shifts with fast rise time were demonstrated in a plasma filled diode experiment. The high sensitivity and vibration isolation enable neutral gas distribution measurements from supersonic nozzles used in plasma radiation source experiments. Examples of these measurements and future applications are described. © 1997 American Institute of Physics. [S0034-6748(97)60001-5]

## I. INTRODUCTION

A high-sensitivity, two-color interferometer was designed and built by Science Research Laboratory (SRL) and installed on the Hawk pulsed power generator at the Naval Research Laboratory (NRL). Two-color interferometry is often used in fusion plasma experiments to subtract phase shifts from vibrations.<sup>1</sup> In many pulsed power experiments, the time scale is 1 ms or less, making vibrational phase shifts negligible, or only a linear ramp that can be subtracted. The two-color feature is used here to simultaneously measure electron and neutral densities.<sup>2</sup> The combination of high phase sensitivity ( $10^{-5}$  wave), high bandwidth (3 ns rise time), and simultaneous phase measurement at two wavelengths make this a unique instrument for diagnosing plasmas and neutrals in pulsed power experiments.

In this article the instrument will be described in general, and examples of measurements at NRL will be given to illustrate three features: simultaneous electron/neutral density discrimination, highly sensitive plasma density measurements, and neutral gas density measurements. A more detailed optomechanical description of the instrument is available.<sup>3</sup>

## II. INTERFEROMETER DESCRIPTION

Figure 1 is a drawing of the instrument as installed on the Hawk plasma opening switch (POS) experiment. The instrument consists of two, independent, equal-path, Mach-Zehnder interferometers mounted on a single, lightweight, stiff space frame suspended by springs inside an H-shaped vacuum chamber. The vacuum chamber rests on air pads for isolation from room vibrations. The instrument straddles the Hawk POS so that the probe arms of the interferometers can take line-of-sight paths through the plasma volume. The reference arms of the interferometers pass through the vacuum chamber above the plasma volume. Besides providing a non-

perturbing path for the reference arm, the vacuum chamber also reduces thermal drifts in the space frame and prevents acoustical vibrations from affecting the interferometers. The internal spring suspension decouples floor vibrations from the space frame. Note that small motions of the space frame on its springs do not affect the measurements since the optical path difference for each interferometer is invariant to translations and rotations of the space frame as a single rigid body. Differential thermal expansions in the space frame typically result in fringe shift drift rates of about 0.001 waves per second. Residual energy in the vibrational modes of the space frame also contribute to low frequency fringe shifts with amplitudes of about 0.001 waves. On the microsecond time scales of the experiments, however, these drifts and oscillations appear only as small, linear ramps in the signal base lines.

Figure 2 shows a schematic of the optomechanical design of the instrument. The probe lasers, lenses, and detection photodiodes are mounted in the same laboratory frame as the Hawk POS. The probe beams enter the interferometer along a path parallel to, and in the same direction of, the interferometer probe paths through the plasma. The probe paths through the plasma are thus invariant to translations of the space frame carrying the interferometers. The incoming probe beams are also nearly coaxial with the probe paths. Small rotations of the space frame thus result in very small translations of the probe paths. In practice, these translations are negligible.

Beam division and recombination in the interferometers is accomplished with polarization beam splitters. For each interferometer the incoming beam is polarized at a nominal  $45^\circ$  to obtain equal intensities in the probe and reference paths after the division. The input focusing lens produces a probe beam waist at the middle of the plasma to be probed. A second polarizing beam splitter at the output of each Mach-Zehnder interferometer combines the probe and reference beams onto a common path. Interference does not occur at this point since the beams are perpendicularly polarized. The two output beams from each interferometer are then

<sup>a)</sup>The abstract for this article was published in *Rev. Sci. Instrum.* **68**, 717 (1997).

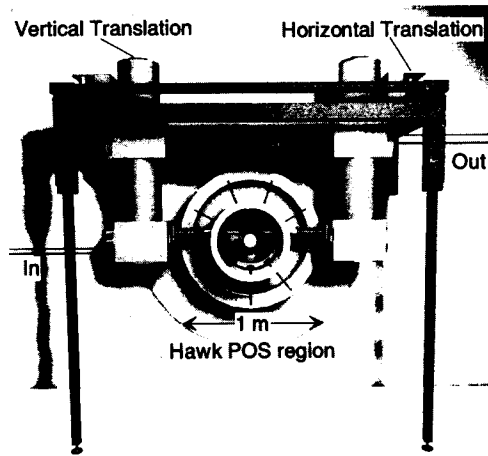


FIG. 1. High sensitivity, two-color interferometer installed on the Hawk generator at NRL.

transported along this common path to the detection optics and electronics located in a screen room some 20 m away. A long focus lens in this path images the beam waist within the plasma onto the detectors to reduce the effects of small refractive deflections of the probe beam within the plasma. A pair of polarization cubes serves as an analyzer to provide

two, complementary, interference fringe patterns centered on two, large area, fast photodiodes in a differential detection circuit. Air turbulence along the path to the detection system does not contribute to the difference signal since the two beams follow a common path. All of the information is transmitted optically into the screen room which allows the detection of small phase shifts isolated from the high electrical noise environment. A similar interferometer design has been described previously.<sup>4</sup>

The interferometer optics are adjusted so that the output beams are coaxial at the output of the interferometer (the zero fringe condition). In this case the laser intensity at the two detectors are proportional to  $a + b \sin(\phi_s + \phi_0)$  on one and  $a - b \sin(\phi_s + \phi_0)$  on the other. Here  $a$  and  $b$  are constants,  $\phi_s$  is the signal phase shift and  $\phi_0$  is a (nominally constant) phase shift which depends on the relative paths within the interferometer. The two detection photodiodes are connected in series with a  $50 \Omega$  load resistor to ground at their common junction. Only their difference current, proportional to  $\sin(\phi_s + \phi_0)$ , flows into the detection electronics. To measure small phase shifts, a piezoelectric translator (PZT) adjusts  $\phi_0$  to zero so that the output signal is proportional to  $\sin(\phi_s)$ . The PZTs also provide calibration by using them to linearly sweep the path difference through several waves to determine the fringe-shift-to-voltage transfer characteristic.

The probe lasers used in this instrument are a Coherent DPSS-532-50 diode-pumped YAG laser providing 50 mW at 532 nm and a Coherent DPSS-1064-100 diode-pumped YAG laser providing 100 mW at 1064 nm. The detectors are EG&G SGD-444 photodiodes with a  $50 \Omega$  load followed by a Stanford Research Systems SR445 wideband preamplifier with gains of  $5\times$ ,  $25\times$ , or  $125\times$ . The data are digitized at 1 G sample/s with a Lecroy 7200 digital oscilloscope with a 2 channel, 8 bit, 7242 digitizing plug in. With this level of laser power, and typical losses in the optical train, the instrument produces a peak difference signal of about 1 V for the 1064 nm probe and 300 mV for the 532 nm probe. For small fringe shifts this corresponds to about 6 V/wave and 2 V/wave, respectively, before amplification. The limiting sensitivity in practice,<sup>3</sup> including shot noise on the photocurrent and thermal noise in the amplifiers, is about  $10^{-5}$  waves, corresponding to a line-integrated electron density of  $2 \times 10^{12} \text{ cm}^{-2}$  for the 1064 nm probe beam.

The primary limitation on this particular system is that the measurement path must be on a line-of-sight through the plasma with no reflections off mirrors attached to the laboratory reference frame. For experiments where the fringe shifts due to neutral species are negligible it would be possible to use the two color analysis to correct for small vibrations in external mirrors instead (which are equivalent to a neutral density shift). The SRL has also used the output signal from the detection electronics as an error signal in a feedback loop with the PZT's to remove low frequency, vibration-induced fringe shifts.

### III. EXAMPLES OF DENSITY MEASUREMENTS IN PULSED POWER EXPERIMENTS

The main features of this interferometer are illustrated by measurements in two pulsed power experiments. Simul-

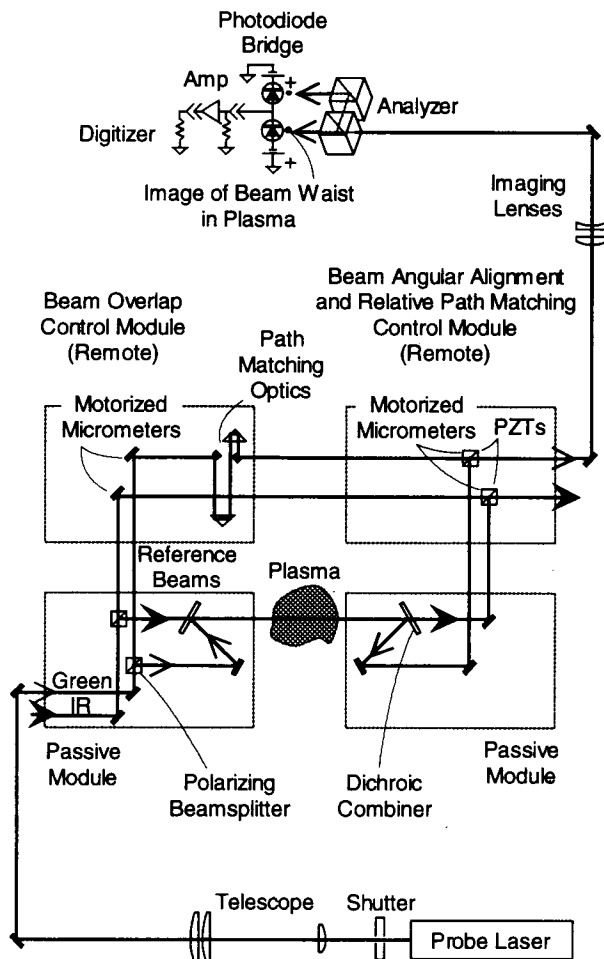


FIG. 2. Schematic of the optomechanical design.

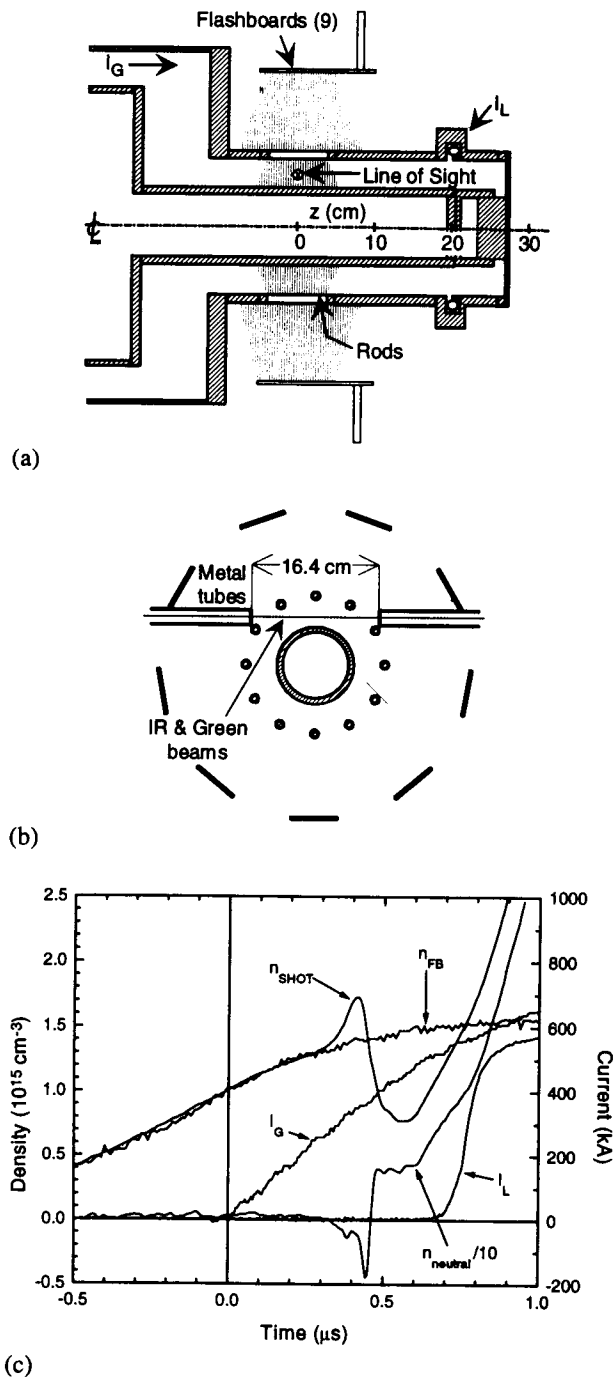


FIG. 3. (a) Cross section of the Hawk POS experiment; (b) chordal line-of-sight in the Hawk POS plasma injection region; (c) measurement results.

taneous plasma and neutral measurements are shown for Hawk POS experiments. High sensitivity electron density measurements are shown for Hawk plasma filled diode (PFD) experiments. High sensitivity neutral measurements are illustrated by plasma radiation source (PRS) nozzle gas distribution measurements.

### A. Measurements of electron and neutral densities in Hawk POS experiment

Figure 3(a) depicts a POS experiment<sup>5</sup> on Hawk. Hawk consists of a high-current Marx bank and a coaxial vacuum output line. The current wave form is sinusoidal with a 700

kA amplitude and a 1.2  $\mu\text{s}$  quarter period. Plasma is injected from flashboard plasma sources<sup>6</sup> into the coaxial line, initially connecting the inner and outer conductors with a highly conducting plasma. When the injected plasma density is about  $10^{15} \text{ cm}^{-3}$ , the plasma conducts the generator current like a short circuit until the current exceeds 500–600 kA, then the current is rapidly switched to a downstream load. [In Fig. 3(a), the load is a shorted electron beam diode.] The plasma density during current conduction and opening has been diagnosed previously<sup>7</sup> using a single color, heterodyne He-Ne interferometer<sup>8</sup> using both axial and chordal lines-of-sight. Two-color interferometry allows simultaneous measurement of electron and neutral densities.

The phase shift due to plasma electrons,  $\phi_e$ , is related to the line-integrated electron number density,  $n_e L$ , by

$$\phi_e = -r_e \lambda n_e L, \quad (1)$$

where  $r_e = 2.82 \times 10^{-13} \text{ cm}$  is the classical radius of the electron and  $\lambda$  is the laser wavelength. The phase shift is negative because the effective index of refraction is less than one. The phase shift from neutrals (or more generally, from any bound electrons in neutrals or ions) is related to the line-integrated neutral number density,  $\rho L$ , by

$$\phi_n = \frac{2\pi\beta}{\lambda} \frac{\rho}{\rho_0} \rho L, \quad (2)$$

where  $\beta$  (the Gladstone-Dale constant) is related to the index of refraction,  $\mu$ , by  $\beta = \mu - 1$  specified at density  $\rho_0$  for the given neutral species. In general, the measured phase shift is the sum of electron and neutral phase shifts. By measuring the phase shift at two wavelengths, the line-integrated electron and neutral densities can be calculated by combining Eqs. (1) and (2), assuming  $\beta$  is independent of wavelength:

$$n_e L = \frac{1}{r_e} \frac{\phi_I \lambda_I - \phi_G \lambda_G}{\lambda_G^2 - \lambda_I^2},$$

$$\rho L = \frac{\rho_0}{2\pi\beta} \frac{\phi_I \lambda_G - \phi_G \lambda_I}{\lambda_G / \lambda_I - \lambda_I / \lambda_G}, \quad (3)$$

where  $\phi_I(\lambda_I)$  and  $\phi_G(\lambda_G)$  are the infrared and green phase shifts (wavelengths).

The chordal line-of-sight through the axial center of the plasma injection region is illustrated in Fig. 3(b). Metal tubes shield the beams from plasma outside the POS region. The path length is 16.4 cm. An example measurement for this experiment is shown in Fig. 3(c). The plasma density measured by firing the plasma sources only,  $n_{FB}$ , rises slowly with time. No measurable neutral density is detected during this time period. When Hawk is fired, the generator current,  $I_G$ , increases to 500 kA in 0.7  $\mu\text{s}$  while the POS is closed. The (short circuit) load current,  $I_L$ , then increases to 500 kA in 0.1  $\mu\text{s}$  when the POS opens. The electron density,  $n_{SHOT}$  (normalized using the 16.4 cm path length) follows  $n_{FB}$  for the first 0.3  $\mu\text{s}$  of the conduction phase, then it increases above and decreases below  $n_{FB}$  as a density shock (snow-plow) moves past the beams.

A large neutral density,  $n_{neutral}$  in Fig. 3(c), is detected, coincident with the time of the density shock. The neutral density eventually becomes much larger than the electron

density. The neutral density is calculated assuming  $\beta$  for carbon atoms in the ground state in Eq. (3). Carbon ions are the most common species in the flashback plasma.<sup>9</sup> The source of the neutrals is probably a combination of charge-exchange neutrals from the flashback plasma, electrode material vaporized by the high current density, and material from the metal shield tubes. The absolute value of the neutral density depends on the species present, but for most species expected in the POS discharge (H,C,O,N), the  $\beta$  values are within a factor of two. The precise value of  $\beta$  does not affect the electron density calculated using the two color method [Eq. (3)], so the technique accurately corrects the electron density for phase shifts caused by neutrals.

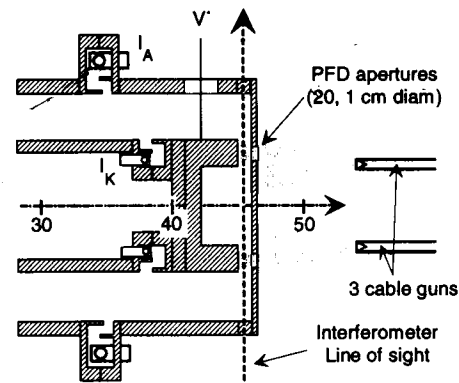
Between  $t=0.4$  and  $0.5 \mu\text{s}$  in Fig. 3(c), the neutral density is negative. This erroneous result could have several causes, including detector time response differences, refractive bending, and species with anomalous dispersion. The photodiode detectors used for these measurements have a slightly different time response, so the differences calculated using Eq. (3) result in large errors when the phase changes quickly. Refractive bending of the probe laser beams by perpendicular density gradients can also affect the calculated neutral density. The imaging lenses (Fig. 2) keep the beams focused on the detectors, but a small tilt will occur that affects the calculated phase shifts differently for the two wavelengths. The effect on the calculated neutral density could be estimated if the density gradient were known. Test measurements with the reference beam blocked show that refraction, plasma flow, and absorption have no effect on the power transmitted through the plasma leg for either wavelength.

Detector response differences and refraction do not explain the calculated negative densities in all cases. For example, using the same line of sight but firing only the flashboards results in a transient negative density even though the rise time is an order of magnitude slower than during a Hawk shot and the density gradients are much smaller.<sup>3</sup> A more likely explanation is that the probed medium contains a significant amount of a species with a strong absorption line between the two probe wavelengths. One candidate is atomic hydrogen in the first excited state at 656.3 nm. For such neutral species, the refractive index is not independent of wavelength [an assumption in Eq. (3)] and will result in negative inferred neutral densities.

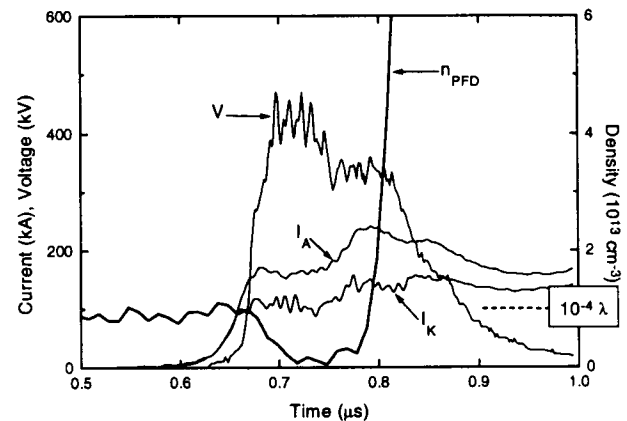
The neutral density measurements in Fig. 3(c) showed that high density neutrals evolve in POS plasmas coincident with the passage of the density shock. The timing and absolute values of the neutral densities have limited accuracy as described above. Improving the absolute accuracy of neutral densities in typical pulsed power experiments using this technique requires knowledge of the species present, detectors with matched time response, and an estimate of refractive effects.

### B. High sensitivity electron density measurement in Hawk PFD experiment

Figure 4(a) is a schematic of a PFD experiment on Hawk that uses the infrared beam of the interferometer to measure low-density plasma dynamics. Plasma is injected into the 10 mm anode-cathode gap prior to the arrival of the Hawk



(a)



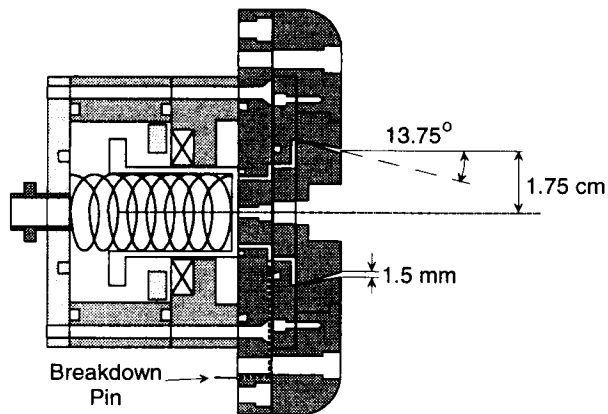
(b)

FIG. 4. (a) Line-of-sight in the PFD experiment on Hawk. (b) Electrical measurements and electron density measured using the infrared beam of the interferometer.

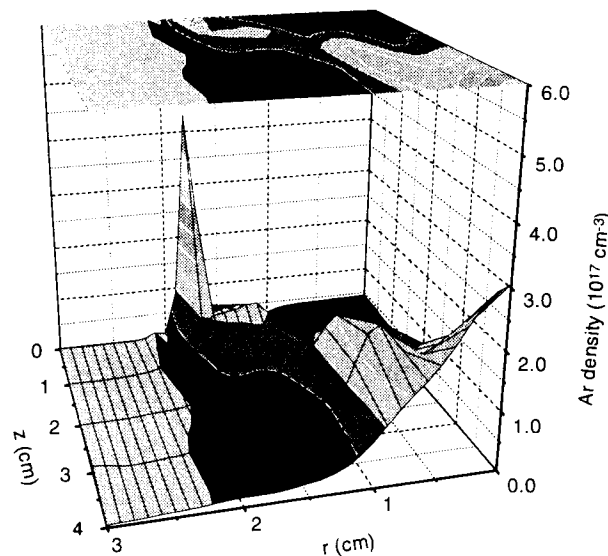
power pulse, using three cable guns. The injected plasma forms a hollow cylinder with a radial thickness of about 1 cm. A POS, located at  $z=0$  [see Fig. 3(a)], provides the fast rising current into the PFD, located at  $z=45$  cm. The interferometer line-of-sight passes through a diameter of the PFD plasma, so the path length is 2 cm.

Measurements with the line-of-sight located 4 mm from the cathode are shown in Fig. 4(b). The Hawk current flows through the POS for  $t < 0.6 \mu\text{s}$ . When the POS opens, current flows through the PFD plasma. Two load current wave forms are shown;  $I_A$  is measured on the anode side of the coaxial line,  $I_K$  is measured on the cathode side. The PFD voltage,  $V$ , is measured with a resistive wire voltmeter. The electrical diagnostics show that the PFD is initially a short circuit that rapidly changes to a  $\sim 3 \Omega$  load impedance. When the voltage increases, the anode and cathode currents separate, indicative of vacuum electron flow. The plasma density, determined using Eq. (1) and the 2 cm plasma length, is about  $1 \times 10^{13} \text{ cm}^{-3}$  before the current flows in the PFD. During the high impedance phase, the density decreases to nearly zero, then increases to a high value. The transient low density indicates a vacuum gap that can support the high voltage pulse. The low density does not persist for the entire high impedance phase, evidence that the gap migrates out of the line-of-sight during the pulse.

The data in Fig. 4(b) illustrate the interferometer's abil-



(a)



(b)

FIG. 5. (a) PRS nozzle used in Phoenix experiments. (b) Abel-inverted gas density profile measured using the green beam of the interferometer.

ity to measure small phase shifts. The phase shift of the 1064 nm beam for an average density of  $1 \times 10^{13} \text{ cm}^{-3}$  and a 2 cm path length is  $10^{-4}$  waves [Eq. (1)]. The minimum density between  $t = 0.7$  and  $0.8 \mu\text{s}$  is about ten times smaller, or  $10^{-5}$  waves.

### C. High sensitivity neutral gas density measurement of PRS nozzle gas distribution

Figure 5(a) is a schematic of a PRS nozzle used on the Phoenix generator at the Naval Surface Warfare Center, White Oak. This nozzle was diagnosed using the green beam of the interferometer to determine the argon gas density distribution during times of interest ( $< 1 \text{ ms}$ ) on Phoenix. The gas flow is supersonic (Mach 4), cylindrical in shape, and tilted inward to decrease the natural radial expansion that leads to zippering<sup>10</sup> in PRSs. The interferometer was used to measure the line-integrated argon density at one location  $(r, z)$  relative to the nozzle, then the nozzle was moved inside the vacuum chamber to scan the  $(r, z)$  cross section. At each location, several pulses were recorded for averaging

and to determine an estimate of the measurement uncertainty. A breakdown pin indicates when gas flows into the nozzle, synchronizing the measurements. The integrated densities are then Abel inverted to determine the density distribution.

The high sensitivity of the interferometer is exploited in this application for measuring small gas densities at large radii. Typically, the dynamic range is 1000 between the highest line density measured along the inner diameter of the gas annulus, and the lowest line density that can be measured relative to vibrational noise that appears to be the limitation on the ms time scale. A typical standard deviation from several sequential measurements is  $5 \times 10^{14} \text{ cm}^{-2}$  which corresponds to a phase shift of  $10^{-4}$  waves [Eq. (2)].

Figure 5(b) is an example of a measured density distribution for this nozzle, at a time relevant for Phoenix PRS experiments (600  $\mu\text{s}$  after the breakdown pin). Measurements were made in axial increments of 1 cm, and in varying radial increments from  $r = 0$  to the radial location where the density decreased below the detection level. The Abel-inverted density distribution in Fig. 5(b) shows a hollow cylinder with argon density greater than  $4 \times 10^{17} \text{ cm}^{-3}$  close to the nozzle exit ( $z = 0$ ). There is a surprisingly high density,  $5 \times 10^{16} \text{ cm}^{-3}$ , on axis ( $r = 0$ ) close to the nozzle, possibly the result of turbulence or boundary layer effects. Far from the nozzle,  $z = 4 \text{ cm}$ , the gas distribution is peaked on axis, a consequence of the inward tilt that successfully maintains the outer radius at about  $r = 2 - 2.5 \text{ cm}$ .

## IV. SUMMARY AND FUTURE WORK

The two-color interferometer described here has been successfully fielded on several pulsed power experiments for high sensitivity measurements of plasma and neutral densities. Electron and neutral densities can generally be distinguished in POS experiments, except when transient species add dispersion that is not independent of wavelength. In cases where the phase shift is dominated by plasma, such as the PFD experiment described above, the infrared beam can measure line-integrated electron densities as low as  $2 \times 10^{12} \text{ cm}^{-2}$ , corresponding to a phase shift of  $10^{-5}$  waves. The green beam can measure phase shifts for supersonic gas flows from PRS nozzles to determine the gas distribution with high precision. These measurements are important for understanding the complex plasma phenomena involved in POS and PFD devices, and for benchmarking hydrodynamic codes that model supersonic gas flows from PRS nozzles.

In the future, high sensitivity two-color interferometry can be applied to different experiments. The electron density will be measured when a high-current (100 kA), MeV proton beam from the Gamble II generator at the NRL interacts with a low pressure (mTorr) gas. This work is in support of the Light Ion Beam ICF Program at Sandia National Laboratories. The successful POS and PFD measurements described above indicate that it may be possible to make a direct measurement of the gap in a parallel plate POS, where the horizontal line of sight can be directed through the low density region as in the PFD experiment. In PRS experiments,

preionization by UV or plasma sources could be diagnosed, and the initial stages of a PRS implosion could be measured.

## ACKNOWLEDGMENTS

The authors thank Dr. M. Krishnan for originally suggesting this work, and Captain D. Massman of DNA for his support throughout the development and installation of the interferometer on Hawk. J. Freshman and F. Yee of SRL made invaluable contributions to the mechanical and electrical design of the interferometer. M. Sucky of JAYCOR provided expert technical assistance on the Hawk experiments. Dr. G. Peterson of NRL made many contributions to the Phoenix PRS nozzle measurements. Dr. R. Riley of NRL provided analyses of the two-color responses of different species. This work was supported by the Defense Nuclear Energy.

- <sup>1</sup>J. H. Irby, E. S. Marmor, E. Sevilano, and S. M. Wolfe, *Rev. Sci. Instrum.* **59**, 1568 (1988); P. Innocente and S. Martini, *ibid.* **59**, 1571 (1988); T. Lehecka, W. A. Peebles, and N. C. Luhmann, Jr., *ibid.* **59**, 1580 (1988).
- <sup>2</sup>R. A. Alpher and D. R. White, *Plasma Diagnostic Techniques*, edited by R. Huddleston and S. Leonard (Academic, New York, 1965), p. 441.
- <sup>3</sup>S. F. Fulghum, Science Research Laboratory, Defense Nuclear Agency Technical Report DNA-TR-93-147, June 1994 (unclassified).
- <sup>4</sup>S. F. Fulghum and M. M. Tilleman, *J. Opt. Soc. Am. B* **8**, 2401 (1991).
- <sup>5</sup>R. J. Commisso, P. J. Goodrich, J. M. Grossmann, D. D. Hinshelwood, P. F. Ottinger, and B. V. Weber, *Phys. Fluids B* **4**, 2368 (1992).
- <sup>6</sup>D. G. Colombant and B. V. Weber, *IEEE Trans. Plasma Sci.* **PS-15**, 741 (1987).
- <sup>7</sup>D. D. Hinshelwood, B. V. Weber, J. M. Grossmann, and R. J. Commisso, *Phys. Rev. Lett.* **68**, 3567 (1992).
- <sup>8</sup>B. V. Weber and D. D. Hinshelwood, *Rev. Sci. Instrum.* **63**, 5199 (1992).
- <sup>9</sup>A. B.-A. Baranga, N. Qi, and D. A. Hammer, *IEEE Trans. Plasma Sci.* **PS-20**, 562 (1992).
- <sup>10</sup>C. Deeney, P. D. LePell, F. L. Cochran, M. C. Coulter, K. G. Whitney, and J. Davis, *Phys. Fluids B* **5**, 992 (1993).